Analyst

ROYAL SOCIETY OF CHEMISTRY

PAPER

View Article Online
View Journal | View Issue

Cite this: *Analyst*, 2021, **146**, 6981

High sensitivity infrared spectroscopy with a diamond waveguide on aluminium nitride

Pontus Forsberg, *[a] Patrik Hollman[b] and Mikael Karlsson *[a]

Mid-infrared waveguide spectroscopy promises highly sensitive detection and characterization of organic molecules. Different material combinations for waveguides and cladding have been demonstrated with promising results, each with its own strengths and weaknesses in terms of sensitivity, transmission window and robustness. In this article we present a 5 μm thick diamond planar waveguide on aluminium nitride cladding, using a new fabrication and polishing method. Diamond has a very wide transmission window in the infrared, and its hardness and high chemical stability allows for chemistries and cleaning protocols that may damage other materials. With an aluminium nitride cladding the waveguide has a useable range between 1000 and 1900 cm^{-1}, which we demonstrate using a tunable quantum cascade laser (QCL). This is a large improvement over silicon dioxide cladding. Compared to previously demonstrated free-standing diamond waveguides, the robustness of the sensor is greatly improved, which allows for a thinner diamond layer and increased sensitivity. The new waveguide was used in a QCL-based optical setup to detect acetone in deuterium oxide and isopropyl alcohol in water. The measurements showed higher sensitivity and lower noise level than previous demonstrations of mid-infrared diamond waveguides, resulting in a two orders of magnitude lower detectable concentration.

Received 7th June 2021,
Accepted 8th October 2021

DOI: 10.1039/d1an01009c

rsc.li/analyst

Introduction

In spectroscopy the term mid-infrared (mid-IR) typically covers a spectral region between 400 and 4000 cm^{-1}. Within this band there are many absorptions related to molecular vibrations, which are useful for identification of substances. In particular, organic molecules have characteristic spectra in the mid-IR. Mid-IR spectroscopy has therefore found applications in a wide range of academic and applied fields, from entomology[1] to medicine,[2] and from food safety[3] to monitoring of greenhouse gases.[4] Of particular interest, considering the COVID-19 pandemic at the time of writing this paper, is the identification of viral infections[5] and specifically COVID-19.[6]

A commonly used technique in mid-IR spectroscopy is attenuated total reflection (ATR). Light is reflected off the inside surface of a high refractive index material at an angle that produces total reflection. Absorption from a lower index sample on the other side of the interface is possible due to the evanescent wave formed during the reflection. As the evanescent wave in the mid-IR typically only reaches a few hundred nanometers to a couple of micrometers into the sample, ATR spectroscopy is an inherently surface sensitive technique. Another advantage of ATR spectroscopy is that liquids, powders, and solids can be analyzed with very little preparation, since the beam path inside the internal reflection element (IRE) is not affected by the sample placed on the surface. ATR spectroscopy can be done with a single reflection, but to increase sensitivity multiple reflections are often used. At the extreme end of this is spectroscopy on a waveguide, with a continuous evanescent wave in contact with the sample (Fig. 1).[7]

Many common optical materials for visible wavelengths and the near-infrared – such as silicon, silicon dioxide (SiO_2), and sapphire – are not transparent in large parts of the mid-IR region. There are however still many materials to choose from,

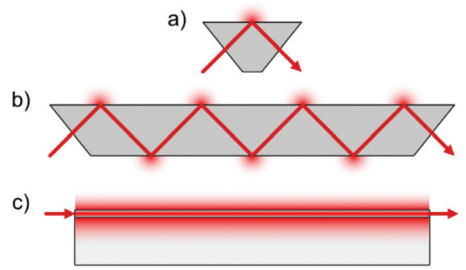

Fig. 1 Illustration of evanescent field on (a) a single reflection IRE, (b) a multiple reflection IRE, and (c) a waveguide on a substrate (cladding). Note that in the waveguide case, the evanescent field extends into the substrate as well as above the waveguide.

[a]*Department of Materials Science and Engineering, Uppsala University, Box 35, 751 03 Uppsala, Sweden. E-mail: pontus.forsberg@angstrom.uu.se, mikael.karlsson@angstrom.uu.se*
[b]*Nova Diamant AB, Tryffelvägen 17, 756 46 Uppsala, Sweden*

all with their own advantages and drawbacks in terms of transparency window, refractive index, stability, ease of processing, and toxicity. Two promising platforms for mid-IR waveguide spectroscopy that have been demonstrated in recent years are gallium arsenide on aluminium gallium arsenide[8] and germanium on silicon.[9] Together with tunable quantum cascade lasers (QCLs) as the light source, both have been shown to have similar capabilities as commercial systems for Fourier transform infrared (FTIR) spectroscopy using ATR. Other waveguide materials that have been used for mid-IR spectroscopy include chalcogenides such as Ge–As–Se on Ge–As–S,[10] different proportions of Ge–Sb–Se,[11] and Hg–Cd–Te on Cd–Te.[12] For the short wavelength end of the mid-IR (below ~4 μm), SiO_2 and sapphire have been used as cladding for ZnSe and Si waveguides.[13–15] For a review of mid-IR spectroscopy using waveguides, see for example Mittal *et al.*[16] or Sieger and Mizaikoff.[17]

Diamond is an interesting material for mid-IR waveguides due to its transparency, comparatively low refractive index (2.38),[18] and extreme hardness and chemical stability. A low refractive index may be desirable because the penetration depth of the evanescent field increases as the difference in refractive index across the interface declines. Diamond has a very wide transparency window from the middle ultraviolet to the far infrared, but there is a band of moderate absorption around 2000 cm^{-1} due to two-phonon interactions.[19,20] The high stability allows for measurements in corrosive environments as well as surface treatments and cleaning procedures that may damage other materials. Diamond surfaces can be functionalized to bind an analyte to the surface.[21] Due to the surface sensitive nature of the evanescent wave, this can vastly enhance the sensitivity of the measurement.

While mid-IR diamond waveguides have been demonstrated for spectroscopy, these have been either free-standing[22,23] or used SiO_2 as cladding.[24] The free-standing waveguides are very fragile, breaking easily with repeated measurements and cleaning. Robustness could be increased by suspending a membrane rather than a single strip; such waveguides have been demonstrated for shorter wavelengths[25] and suggested for the mid-IR.[26] For a waveguide that can stand up to physical cleaning though (*e.g.* to scrub away dried in proteins), the mechanical support of a solid substrate is desirable. An interesting way to produce diamond waveguides that has been demonstrated in recent years is to partially graphitize bulk diamond with a femtosecond laser, thereby inducing stresses that modify the refractive index.[27–29] Such waveguides have been demonstrated to work in the mid-IR,[30] and if produced close enough to the surface, may in the future be suitable for spectroscopy. A more traditional approach, using a solid cladding layer, is somewhat challenging with diamond. A cladding material with a lower refractive index is required and diamond has a low refractive index compared to most other materials transparent in the 5–10 μm wavelength range. A waveguide with a high sensitivity to analytes will typically also be sensitive to absorption in the cladding. SiO_2 cladding can be used, but is strongly absorbing at longer wavelengths. Based on our own preliminary experiments, a 10 mm long and 15 μm thick (resulting in low sensitivity) diamond on SiO_2 waveguide coupled with a strong light source, such as a tunable QCL, could be used for measurements down to around 1300 cm^{-1} (7.7 μm). According to Kischkat *et al.*,[31] the extinction coefficient of SiO_2 at this wavenumber is 0.039. Aluminium nitride (AlN), on the other hand, does not reach a similar value for the extinction coefficient until 1050 cm^{-1} (9.5 μm).[31] AlN has previously been demonstrated as a cladding layer for diamond waveguides at near-IR wavelengths,[32] and suggested as a cladding material for thick waveguides in the wavelength range 7.7 to 13.7 μm.[33] Here we present a diamond slab waveguide with AlN cladding, fabricated using a new method, and demonstrate its use for sensitive mid-IR spectroscopy. To our knowledge, this is the first experimental demonstration of a diamond on AlN waveguide for mid-IR wavelengths, and the first use of such a waveguide for measuring an analyte. A robust cladding layer with low absorption allowed us to use a thinner waveguide than previously demonstrated for mid-IR spectroscopy, which resulted in higher sensitivity.

Experimental

Waveguide fabrication

While diamond can be deposited directly on AlN,[34] this would have required a time-consuming optimization process. Depositing diamond on Si and then moving it to AlN allowed the use of a well-tested deposition process for a film of high optical quality. The transfer was accomplished by sputtering AlN onto the diamond film, gluing this to a new substrate, polishing the edges, and then etching away the Si growth substrate.

The 5.0 μm thick polycrystalline diamond film of optical grade used for the waveguide was deposited by Chemical Vapor Deposition (CVD) on a silicon wafer and polished to a less than 10 nm arithmetical mean roughness (Ra) by Diamond Materials GmbH. The wafer was laser cut to produce 5 mm × 10 mm samples. AlN was deposited on the diamond by reactive sputtering from an Al target in a Von Ardenne magnetron sputter system. The process parameters were: 900 W pulsed DC power, 2 mTorr pressure, 15 sccm argon and 45 sccm nitrogen gas flows. A more detailed account of the sputter system and process has been published previously.[35] In order to keep the substrate temperature low, the sputtering was done in four cycles of 30 minutes with the machine left to cool down to room temperature between cycles. This was found to be necessary to avoid cracking and peeling of the AlN film. Each cycle resulted in a film thickness of 0.9 μm for a total thickness of 3.6 μm. A piece of 1 mm thick glass was cut to 5 mm × 10 mm size and glued on top of the silicon/diamond/AlN stack using a heat curing epoxy resin (EPO-TEK 353ND). The edges of the diamond film were mechanically polished using a CVD diamond coated polishing wheel developed by Nova Diamant AB, resulting in around 3 nm Ra rough-

ness (as measured by a ZYGO NexView NX2 optical profiler) with only occasional pits up to a few tens of nm deep. By polishing the edges while the diamond film was supported from both sides, the risk of cracking was reduced. Polishing served to smoothen the rough laser cut edges of the diamond film and also removed any AlN, epoxy and silicon (redeposited during laser cutting) from the edges. Mechanical polishing produced smoother end faces than the plasma etching and focused ion beam milling that we have used on previous diamond waveguides,[22–24] and preliminary tests showed greatly improved coupling of light through the waveguides. Finally, the original silicon substrate was removed by dry etching with argon and sulfur hexafluoride in an inductively coupled plasma etcher (PlasmaTherm SLR). The etch process leaves the diamond surface fluorine terminated, making it hydrophobic.[36]

For comparison, a diamond IRE was also evaluated. This solid polycrystalline element of optical grade diamond was manufactured by Diamond Materials GmbH and had the dimensions 15 mm × 12 mm × 0.45 mm with the shorter edges at a 45° angle.

Optical testing

A tunable QCL was used to test the waveguide (MIRcat system from Daylight Solutions). This laser produces a beam that is predominantly (100 : 1) vertically polarized, meaning we will excite transverse magnetic (TM) modes in the waveguide. The mode profiles at 1600 cm^{-1} calculated using a 1-D mode solver[37] with a 5 μm diamond waveguide between an AlN cladding and water analyte are shown in Fig. 2. A 2-D finite difference time domain simulation with Meep[38] of such a waveguide, using a 5 μm Gaussian beam as the input, produced an average squared E-field identical to the profile of the TM_0 mode in Fig. 2. The TM_1 mode is close to anti-symmetric, and as such is barely excited by the symmetric Gaussian beam.

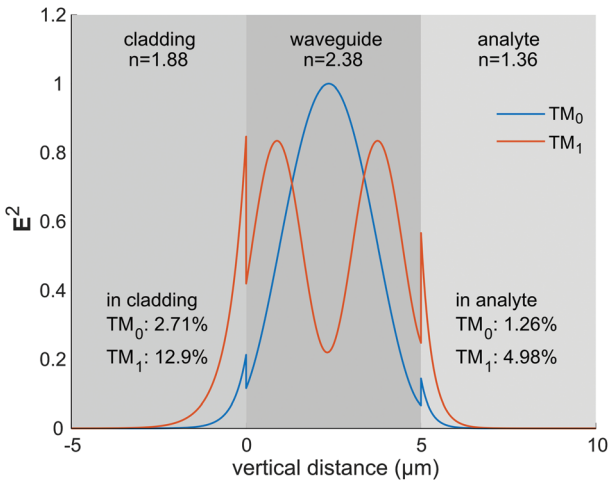

Fig. 2 Mode profiles of TM modes at 1600 cm^{-1} of a 5 μm thick diamond waveguide on AlN with water analyte. Refractive indices of AlN, diamond and water taken from the literature.[18,31,39]

While the input in our experiments is not a perfect Gaussian beam, we expect very little light is coupled into the higher mode. The higher mode will also be absorbed quicker due to the greater evanescent field.

The setup used to test the waveguides is shown schematically in Fig. 3. The beam from a tunable mid-IR laser was guided by two gold mirrors and focused by a 12.5 mm germanium lens onto the end of the waveguide or IRE. On the detector side, the light was gathered by a 12.7 mm zinc selenide lens and finally focused by a 25 mm zinc selenide lens onto a thermoelectrically cooled MCT (mercury cadmium telluride) detector (PVMI-4TE-12 from VIGO System SA). When necessary, an iris before the first focusing lens was used to reduce the intensity on the detector. This was only the case when measuring with the IRE or free space. An oscilloscope (National Instruments PXIe-5114) was used to capture the signal from the detector as well as trigger signals from the laser; a computer running LabView controlled the laser and oscilloscope to collect the spectra.

The laser system contains four QCL modules covering a spectrum between approximately 1900 and 900 cm^{-1}. The laser was operating in pulsed mode with a pulse frequency of 100 kHz and a pulse length of 400 ns. To record a spectrum, a QCL module was scanned across its range with scan speed set to 20 cm^{-1} s^{-1} while the oscilloscope saved a record at a trigger signal from the laser every 0.5 cm^{-1}. The record length from the oscilloscope was 200 000 points with a sample rate of 125 MHz, resulting in a recorded time of 1.6 ms containing about 160 pulses. The output was calculated as the difference between the mean voltage during the pulses and the mean voltage between pulses. The QCL-modules were not perfectly aligned with each other and the spectrum also varied somewhat across the beam spot. Because of this, the shape of the spectrum and the relative intensity between the QCL-modules depended on the alignment of the optical set-up, especially the iris and the positioning of the waveguide.

Propagation losses were measured by passing light through the waveguide along both the shorter (5 mm) and longer (10 mm) dimension of the waveguide. Assuming coupling losses to remain the same, the propagation loss in dB cm^{-1} is

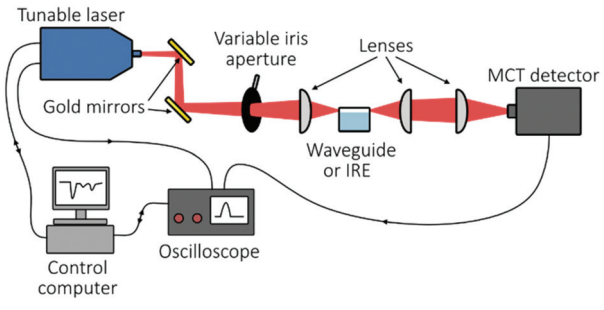

Fig. 3 Schematic view of the measurement setup. The iris was used in the IRE measurements and when measuring the spectrum directly from the laser, so that the detector could work in a range where the output is linear.

straightforward to calculate as $-20 \times \log_{10}(V_{10}/V_5)$, where V_{10} and V_5 are the measured outputs with 10- and 5 mm waveguide respectively. Focus and position was adjusted for each measurement to maximize the signal on the detector, and the measurements were repeated three times for each wavelength.

Absorption spectra were measured using low concentrations of isopropyl alcohol (IPA) in water and acetone in deuterium oxide (D_2O). The IPA spectra were measured in the range of QCL-3 (see Fig. 4b), and acetone in the range of QCL-2. Acetone in D_2O was chosen to enable comparison with a previous diamond waveguide.[22] The concentrations used were 0.2, 0.5, 1, 2, 5 and 10 vol% IPA in water (or 26, 66, 130, 260, 660 and 1300 mmol L^{-1}), and 0.05, 0.2, 0.5, 1, 2, and 5 vol% acetone in D_2O (6.7, 27, 68, 140, 270 and 680 mmol L^{-1}). For all waveguide spectra, the 5 mm dimension of the waveguide was used. The results were compared with those from the 15 mm long multi-reflection diamond IRE using the same QCL setup (not all of the concentrations of acetone in D_2O were measured on the IRE).

For the measurements, a 50 μl droplet was placed on top of the waveguide. The droplet completely covered the 5 mm length of the waveguide, while the hydrophobicity of the fluorine terminated diamond surface prevented wetting of the edges. The liquid also served to block stray light from going above the waveguide (when measuring with a dry waveguide, stray light was blocked by a piece of filter paper with a small weight to hold it down). On the IRE, the 50 μl droplet spread to a diameter of around 7 mm (corresponding to around 4 reflections in the IRE). The droplet was carefully placed on the center of the IRE, but since it did not cover the whole surface, variations in droplet position was a potential source of error.

Each spectrum was recorded in four groups of five scans. The scan time was 18 s and resetting for the next scan took 14 s, for a total cycle time of 32 s. Between groups, the liquid was removed (by gently wiping with tissue paper and blowing with nitrogen) and five background spectra were measured with pure water or D_2O. Dividing the measurements in this way was done to minimize the effect of drift. If the time between background and sample spectra was more than a few minutes, the slight alignment drift was enough to overshadow the absorptions at the lowest concentrations. To remove occasional large disturbances from the data, up to 5 spectra with large fluctuations were removed before averaging.

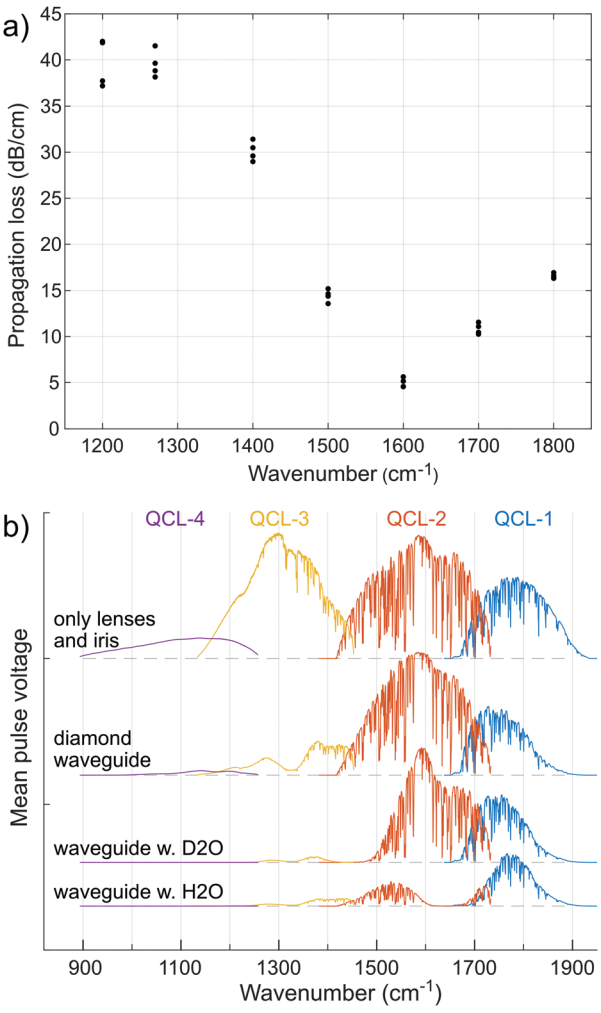

Fig. 4 (a) Propagation losses. (b) Raw spectra with all four QCL-modules in the laser system. The top row is without a waveguide or IRE in the beam path, but with an iris to reduce the intensity (to not saturate the detector). The lower three rows were recorded with the diamond waveguide. From the top, they are dry (with filter paper to block light over the guide), pure D_2O, and pure water on top. The spectra have been rescaled to allow all the spectra to be seen and compared.

Results

The measured propagation losses in the waveguide can be seen in Fig. 4a. At high wavenumbers there is some absorption in the diamond due to the 2-phonon absorption. As we go to low wavenumbers we instead see increasing absorption in the AlN cladding, and below 1200 cm^{-1} we did not get enough signal through the 10 mm waveguide length to make a reliable loss measurement. In between, there is a sweet spot around 1600 cm^{-1} where the propagation losses are as low as 5 dB cm^{-1}. Fig. 4b shows raw spectra of the laser without a waveguide, with the waveguide, and with water and D_2O on the waveguide. When measuring the spectra without a waveguide, an iris was used to reduce the intensity, so that the detector could work in a range where the response is close to linear. The spectra have a lot of spikes above ~1300 cm^{-1} due to absorption by water vapor in the beam path. By comparing their positions to published water vapor spectra,[40,41] we could calibrate the wavenumber tuning to within ~1 cm^{-1}. The second row of spectra in Fig. 4b shows spectra with a dry waveguide. Comparing these with the top row we see that the signal drops off more quickly at high wavenumbers (above 1800 cm^{-1}). This is due to the two-phonon absorption band in diamond, with strong absorption between 1800 and 2300 cm^{-1}. From around 1500 cm^{-1} and lower, we see a reduction in the signal, with a dip around 1325 cm^{-1}. The

signal was still strong enough to make some limited measurements down to around 1000 cm^{-1}.

The lower two sets of spectra in Fig. 4b are taken through the waveguide with D_2O and water on top. Both liquids have some absorption in the whole range, especially towards lower wavenumbers, resulting in an even weaker signal. As we will see below, it was possible to make measurements in water down to around 1150 cm^{-1}. With water on the waveguide, the strong absorption around 1640 cm^{-1} reduced the signal to zero. The same thing happened with D_2O around 1450 cm^{-1}, showing that our D_2O has picked up quite a bit of regular water from the atmosphere, since this is where we would expect a HDO (semi-heavy water) absorption.[42] D_2O also has a strong absorption around 1200 cm^{-1}, though the signal was too weak for this to be visible in Fig. 4b.

Note that the vertical scale of the spectra in Fig. 4b has been adjusted to make comparisons of features possible. The absolute values are of little interest, since to produce good spectra the iris was needed to adjust the intensity when the waveguide was not used.

The spectra of IPA in water, acquired using the waveguide and the IRE, are shown in Fig. 5a–c. Some absorptions are shifted from where we find them in pure IPA by up to 8 cm^{-1}, presumably due to interactions with water, but all the absorptions that we expect from IPA are clearly seen.[43] The spectra measured with the IRE required a bit more processing.

Due to a ripple in the signal, these spectra were filtered with a band stop filter. Since the droplet did not cover the whole diamond surface, the size and position could vary somewhat each time the liquid was changed, which led to small differences in overall intensity between background and sample spectra and could introduce a slight slope (since the water absorption declines with wavenumber in this range). To counter this, we also subtracted a line drawn between the values at 1220 and 1440 cm^{-1}, where there is little absorption from IPA. Unfortunately, this hides the effect of lowering water concentration: Where IPA is less absorbing than water, the intensity increases with increasing IPA concentration. This can be seen between 1180 and 1270 cm^{-1} in the waveguide spectra (Fig. 5a).

The much larger thickness of the IRE compared to the waveguide allowed us to focus the whole laser spot on the input face. Together with the absence of a cladding layer and much lower sensitivity, this resulted in a higher light intensity through the IRE, especially at lower wavenumbers. The effect of this in the IPA spectra is a lower absolute noise level in the IRE spectra compared to the waveguide. In the waveguide spectra, the noise is strongest at low wavenumbers, where the power through the waveguide was low. Both sets of spectra are noisy around the water vapor absorptions above 1400 cm^{-1}, but since this did not interfere with the absorptions we are looking at we have not attempted to filter this out. While the noise with the IRE was lower, the signal was also about an order of magnitude smaller. In the end, the spectra are clearer using the waveguide than the IRE. The absorptions around 1310 cm^{-1} and 1390 cm^{-1} are clearly visible even at 0.2% concentration (Fig. 5c) in the waveguide spectrum, in contrast to the IRE spectrum where they are hardly discernible. The

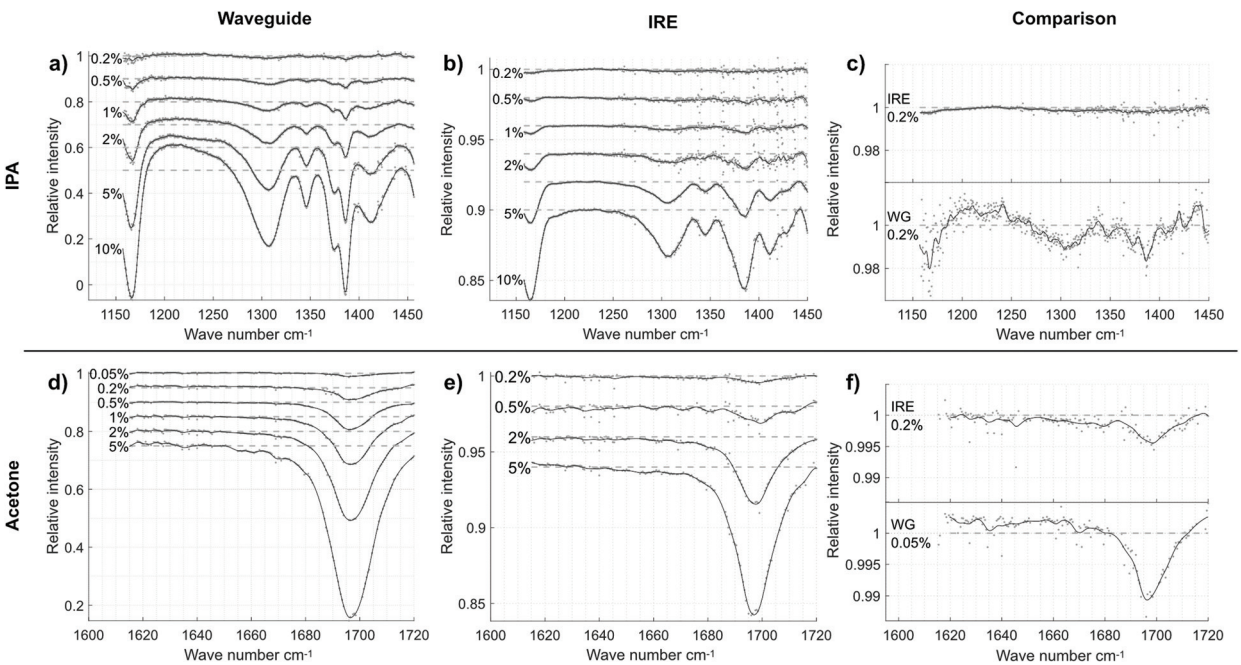

Fig. 5 Spectra of IPA in water (top row) and acetone in D_2O (bottom row), normalized to background spectra of pure water and D_2O respectively. Grey dots represent data points after averaging (in (b) also filtering and straightening). The black lines are smoothing spline fits to the data. The spectra to the left were acquired with the waveguide and those in the center with the IRE. To the right are comparisons of the lowest concentrations measured. Note that the spectra in (a, b, d, and e) have been displaced vertically to not overlap.

absorption between 1360 and 1400 cm^{-1} can be clearly seen as a double "peak" in the waveguide spectra. In the IRE spectra, this feature was lost to filtering, though it is possible that more gentle filtering could preserve it to some extent.

In the spectra of acetone (Fig. 5d–f), the only interesting absorption feature in the range is the strong CO stretch. In pure acetone, we would expect to see this at 1712 cm^{-1}. With low acetone concentrations in water however, hydrogen bonding causes this absorption to shift to where we see it here (1697 cm^{-1}).[44] In this range, the spectra measured using the IRE did not show any interference pattern, so no filtering was necessary. However, the strong absorptions from water vapor resulted in higher levels of noise in all spectra at some wavenumbers. Because of this, points were removed where the standard deviation between background spectra exceeded 3%. The transmission through the waveguide was high enough that the noise levels were similar for the waveguide and IRE. This means that the waveguide with its higher sensitivity comes out well ahead when comparing the absorption at 1697 cm^{-1}. In Fig. 5f we see that even with a concentration a factor 4 lower, the waveguide spectrum is clearer. For the IRE, the absorption is visible at 0.2% concentration, but it is below what we would consider a limit of detection (LOD) by visual evaluation. In the case of the waveguide, it looks like there is still room to reduce the concentration below 0.05% and still be detectable.

Acetone and D_2O are both difficult to measure without a controlled atmosphere or enclosed measurement cell. The concentration of acetone in a small water droplet in air will fall quickly due to evaporation. D_2O on the other hand is highly hygroscopic and will absorb water from the surrounding air. The measurement was started within seconds after placing the droplet, but the cycle time of 32 s per scan was enough to significantly reduce the absorption of acetone and increase the HDO absorption with each scan, as can be seen in Fig. 6 where the scans have been averaged separately. The HDO spectrum has been normalized to the first scan. The acetone absorption goes from more than 70% to about 40% in a little over two minutes.

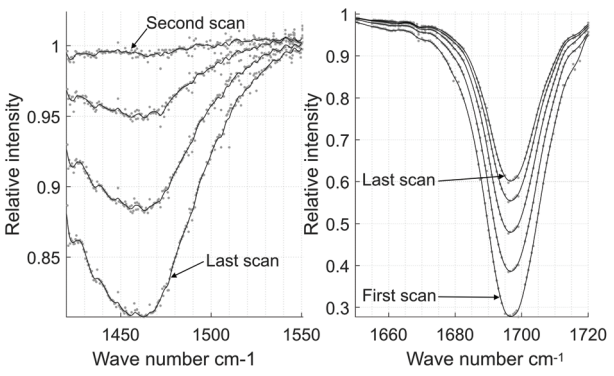

Fig. 6 Acetone and D_2O spectra evolve over time. On the left, the growth of the HDO absorption as water is absorbed from the atmosphere (normalized to the first scan in the sequence). On the right, the reduction in absorption as 5% acetone in D_2O evaporates.

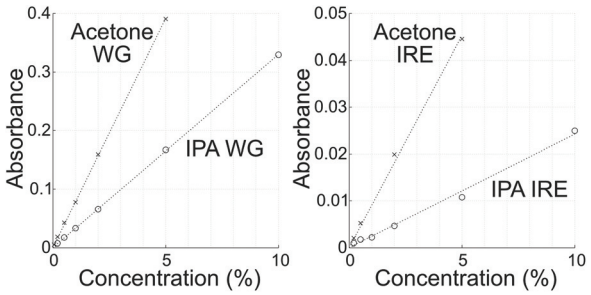

Fig. 7 Absorbance plotted against concentration with linear fits. Measurements with the waveguide are plotted to the left, and with the IRE to the right.

To get a measure of the sensitivity of the waveguide and IRE, absorbance (calculated as $-\log_{10}(T)$, where T is the value of the fitted curve in Fig. 5) is plotted against concentration in Fig. 7 together with linear fits to the data. The IPA absorbance is for the absorption at 1386 cm^{-1}. The LOD can be estimated by LOD = 3.3 × σ/S, where S is the sensitivity (*i.e.* the slope of the linear fit in Fig. 7) and σ is the standard deviation of the y-intercept of the fitted line.[45] The S and σ, as well as goodness of fit (R^2) are given in Table 1 along with the resulting LODs. Note that these LODs are fairly rough estimates, since some of the concentrations measured are more than ten times higher than the calculated LOD.

Discussion

There was detectable transmission through the dry waveguide from around 1000 cm^{-1} to 1900 cm^{-1}. This is the range we would expect based on the known absorptions in the waveguide and cladding materials. A gradual reduction in propagation loss was seen up to around 1600 cm^{-1}, this should be due to the absorption in AlN decreasing,[31] and possibly also the penetration depth decreasing at higher wavenumbers. At the upper end the transmission range is limited by the two-phonon absorption in diamond. There is an unidentified absorption around 1325 cm^{-1}. This could be due to an impurity in the cladding or waveguide (however, it does not look like a nitrogen absorption in diamond). When measuring in aqueous solution with a high sensitivity waveguide, fairly high losses are unavoidable in the range below the strong H_2O bending absorption around 1640 cm^{-1}. Despite higher losses in both the water and the cladding, and the relatively weak absorption peak studied, we achieved almost as low detection limit for IPA in water as for acetone in D_2O. So, while absorption and the resulting propagation loss ultimately limit the usable range of the waveguide, performance can remain stable unless one goes to the very edges of this range (such as the IPA absorption at 1160 cm^{-1}, seen in Fig. 5a and c).

While acetone in D_2O is an attractive model in that it has a strong single absorption in a range that is relevant for many biomolecules, measurement without an enclosed cell or con-

Table 1 Fit parameters and LOD, calculated from the linear fits in fig. 7

	Sensitivity AU/vol% (AU/(mol L^{-1}))	σ AU	R^2	LOD vol% (mmol L^{-1})
IPA WG	3.3×10^{-2} (0.25)	8.3×10^{-4}	0.9999	0.083 (11)
IPA IRE	2.4×10^{-3} (0.019)	6.7×10^{-4}	0.9931	0.90 (120)
Acetone WG	7.8×10^{-2} (0.58)	1.3×10^{-3}	0.9999	0.057 (7.6)
Acetone IRE	8.8×10^{-3} (0.067)	1.8×10^{-3}	0.9978	0.66 (86)

Sensitivity is the slope of the fitted line, σ is the standard deviation of the y-intercept, R^2 is the "goodness of fit". "Absorbance Unit" (AU) is used for the dimensionless absorbance. Molar concentrations are included in parentheses for easier comparison.

trolled atmosphere is time sensitive. The good linear fits to the acetone measurements in Fig. 7 show that consistent measurements could be made despite the rapid evaporation of acetone and hygroscopic nature of D_2O. But from Fig. 6 it is clear that the average concentrations measured are actually below the nominal values. The hygroscopic nature of D_2O is problematic since the HDO and H_2O absorptions affect both the background and sample measurements, making it difficult to fix a baseline for the acetone measurement. This is not much of a problem for a visual inspection; as we saw in Fig. 5f the absorption from of 0.05% acetone could be clearly seen in the spectrum. It does however lead to more uncertainty in the absolute absorbance values, which is reflected in the values of σ in Table 1 being higher for the acetone measurements than for IPA in water.

The waveguide had a sensitivity that was around one order of magnitude greater than that of the IRE. This difference translated to a similar order of magnitude difference in LOD. It should however be noted that our set-up should be optimized further to get maximum sensitivity out of either component. The demonstrated detection limit of around 0.05% acetone with the waveguide is comparable to what can be achieved for ethanol with a high-end ATR-FTIR spectrometer.[46] As has been mentioned above, our measurement set-up still has plenty of room for improvement in terms of stability and atmosphere control. With these in place it is our belief that we will be able to push beyond the limits of ATR-FTIR. Even if the performance remains similar between the systems, they are complementary methods, as a tunable QCL can be operated in ways that FTIR cannot and *vice versa*. Other potential advantages to waveguide spectroscopy compared to ATR-FTIR that have been brought up in the literature are cost benefits (thin films use less material and are suitable for batch fabrication methods) and chip-scale platform integration,[47] although these have yet to be demonstrated in the mid-IR.

Compared to a previously published mid-IR diamond waveguide,[22] the one presented here is thinner (5 μm compared to 14 μm), meaning it could support 2 to 3 TM modes compared to the ~10 modes in the thicker waveguide. This reduced thickness resulted in an increased sensitivity to acetone by about a factor 3 after taking the difference in interaction length into account. Compared to the 6 μm thick gallium arsenide on gallium aluminium arsenide single mode waveguide in the same article,[22] our current diamond waveguide is around 6 times more sensitive. Since we also achieved much lower noise levels, the improvement in detectable concentration was much greater, around two orders of magnitude. The reduction in noise was probably in large part due to improvements in the mechanical stability of the waveguide, control of the interaction length, and signal handling. Another important contributor was the mechanical polishing of the ends of the waveguide, which resulted in smoother surfaces than the plasma etching previously used.

While high sensitivity is desirable in waveguide spectroscopy, it does come with some drawbacks. One is that the sensitivity is high on both sides of a slab waveguide, putting high demands on the transparency of the supporting cladding layer. Another is that the sensitivity will also be high to absorption in the medium that one is looking for a signal in. In Fig. 4b we saw that water reduced the transmission significantly for wavenumbers below 1750 cm^{-1} and for a fairly wide band around 1640 cm^{-1} there was no signal at all. This would require samples to be dried or in a different medium than water to study absorptions in this range. However, high sensitivity is a large part of what sets waveguide spectroscopy apart from regular ATR spectroscopy and makes it a good complementary technique. There is therefore good reason to aim for high sensitivity, even if it does not satisfy every use case.

Conclusions

We have demonstrated a 5 μm thick polycrystalline diamond slab waveguide on AlN cladding. In tests with mixtures of IPA in water and acetone in D_2O, the waveguide showed sensitivity and limit of detection around one order of magnitude higher than a diamond IRE in the same set-up, and 3–6 times higher sensitivity than previously published diamond and GaAs waveguides. Because of this and due to other improvements in the measurement and set-up, LOD was improved by around two orders of magnitude. The AlN cladding supported the waveguide while still allowing for measurements down to about 1150 cm^{-1} in water or 1000 cm^{-1} with a dry waveguide. The improved robustness made this waveguide possible to handle and clean without a high risk of breaking, making it much more practical to use than previous free-standing diamond waveguides despite being thinner.

To further improve the waveguide, transmission should be improved, especially for wavenumbers below ~1450 cm^{-1}. Since the process for putting the diamond film on an AlN clad-

ding has exposed the seed side of the diamond film, it may be possible to improve the quality of the film by etching or polishing away the initial growth layer. The cladding layer also needs improving, we have shown here that AlN gets us further than SiO_2, but trying to optimize the deposition parameters further would be interesting. The process of moving the diamond film from a growth substrate to a different cladding layer also opens up for using cladding materials that are not suited for diamond deposition. Once we have a good enough cladding layer, we will attempt to make single-mode mid-IR waveguide sensors in diamond.

Author contributions

PF – Conceptualization, software, methodology, investigation, visualization, writing – original draft. PH – Methodology, resources, writing – review & editing. MK – Conceptualization, funding acquisition, project administration, resources, methodology, writing – review & editing.

Conflicts of interest

There are no conflicts to declare.

Acknowledgements

The research leading to these results has received funding from the Swedish Research Council (VR, research grant No. 621-2014-5959). Myfab is acknowledged for support and for access to the nanofabrication laboratory at Uppsala University.

Notes and references

1 J. B. Johnson and M. Naiker, *J. Asia-Pac. Entomol.*, 2020, **23**, 613–621.
2 S. De Bruyne, M. M. Speeckaert and J. R. Delanghe, *Crit. Rev. Clin. Lab. Sci.*, 2018, **55**, 1–20.
3 W.-H. Su and D.-W. Sun, *Food Eng. Rev.*, 2019, **11**, 142–158.
4 H. E. Brindley and R. J. Bantges, *Curr. Clim. Change Rep.*, 2016, **2**, 112–126.
5 M. C. D. Santos, C. L. M. Morais and K. M. G. Lima, *Biomed. Spectrosc. Imaging*, 2020, **9**, 103–118.
6 L. Zhang, M. Xiao, Y. Wang, S. Peng, Y. Chen, D. Zhang, D. Zhang, Y. Guo, X. Wang, H. Luo, Q. Zhou and Y. Xu, *Anal. Chem.*, 2021, **93**, 2191–2199.
7 T. Schädle and B. Mizaikoff, *Appl. Spectrosc.*, 2016, **70**, 1625–1638.
8 M. Sieger, J. Haas, M. Jetter, P. Michler, M. Godejohann and B. Mizaikoff, *Anal. Chem.*, 2016, **88**, 2558–2562.
9 V. Mittal, G. Devitt, M. Nedeljkovic, L. G. Carpenter, H. M. H. Chong, J. S. Wilkinson, S. Mahajan and G. Z. Mashanovich, *Biomed. Opt. Express*, 2020, **11**, 4714–4722.
10 P. Ma, D. Y. Choi, Y. Yu, X. Gai, Z. Yang, S. Debbarma, S. Madden and B. Luther-Davies, *Opt. Express*, 2013, **21**, 29927–29937.
11 A. Gutierrez-Arroyo, E. Baudet, L. Bodiou, J. Lemaitre, I. Hardy, F. Faijan, B. Bureau, V. Nazabal and J. Charrier, *Opt. Express*, 2016, **24**, 23109–23117.
12 X. Wang, J. Antoszewski, G. Putrino, W. Lei, L. Faraone and B. Mizaikoff, *Anal. Chem.*, 2013, **85**, 10648–10652.
13 V. Mittal, M. Nedeljkovic, D. J. Rowe, G. S. Murugan and J. S. Wilkinson, *Opt. Lett.*, 2018, **43**, 2913–2916.
14 Y. Qi, D. J. Rowe, V. Mittal, M. Banakar, Y. Wu, M. Nedeljkovic, J. S. Wilkinson and G. Z. Mashanovich, Proc. SPIE, Silicon Photonics XIV, 2019, 10923, 109230I.
15 N. Singh, A. Casas-Bedoya, D. D. Hudson, A. Read, E. Mägi and B. J. Eggleton, *Opt. Lett.*, 2016, **41**, 5776–5779.
16 V. Mittal, G. Z. Mashanovich and J. S. Wilkinson, *Anal. Chem.*, 2020, **92**, 10891–10901.
17 M. Sieger and B. Mizaikoff, *Anal. Chem.*, 2016, **88**, 5562–5573.
18 A. M. Zaitsev, *Optical Properties of Diamond*, Springer-Verlag, Berlin Heidelberg, 2001.
19 P. Dore, A. Nucara, D. Cannavò, G. De Marzi, P. Calvani, A. Marcelli, R. S. Sussmann, A. J. Whitehead, C. N. Dodge, a. J. Krehan and H. J. Peters, *Appl. Opt.*, 1998, **37**, 5731–5736.
20 R. P. Mildren, in *Optical Engineering of Diamond*, ed. R. P. Mildren and J. R. Rabeau, Wiley-VCH Verlag & Co. KGaA, Weinheim, 2013, ch. 1, pp. 1–31.
21 P. O. Andersson, P. Viberg, P. Forsberg, F. Nikolajeff, L. Österlund and M. Karlsson, *Anal. Bioanal. Chem.*, 2016, **408**, 3675–3680.
22 X. Wang, M. Karlsson, P. Forsberg, M. Sieger, F. Nikolajeff, L. Österlund and B. Mizaikoff, *Anal. Chem.*, 2014, **86**, 8136–8141.
23 M. Malmström, M. Karlsson, P. Forsberg, Y. Cai, F. Nikolajeff and F. Laurell, *Opt. Mater. Express*, 2016, **6**, 1286–1295.
24 A. I. López-Lorente, P. Wang, M. Sieger, E. V. Catalan, M. Karlsson, F. Nikolajeff, L. Österlund and B. Mizaikoff, *Phys. Status Solidi A*, 2016, **213**, 2117–2123.
25 A. H. Piracha, P. Rath, K. Ganesan, S. Kühn, W. H. P. Pernice and S. Prawer, *Nano Lett.*, 2016, **16**, 3341–3347.
26 A. T. Rahmati, G. Z. Mashanovich and M. P. Nezhad, *J. Opt.*, 2021, **23**, 075801.
27 B. Sotillo, V. Bharadwaj, J. P. Hadden, M. Sakakura, A. Chiappini, T. T. Fernandez, S. Longhi, O. Jedrkiewicz, Y. Shimotsuma, L. Criante, R. Osellame, G. Galzerano, M. Ferrari, K. Miura, R. Ramponi, P. E. Barclay and S. M. Eaton, *Sci. Rep.*, 2016, **6**, 35566.
28 A. Courvoisier, M. J. Booth and P. S. Salter, *Appl. Phys. Lett.*, 2016, **109**, 031109.
29 H. Hanafi, S. Kroesen, G. Lewes-Malandrakis, C. Nebel, W. H. P. Pernice and C. Denz, *Opt. Mater. Express*, 2019, **9**, 3109–3114.

30 V. Bharadwaj, Y. Wang, T. T. Fernandez, R. Ramponi, S. M. Eaton and G. Galzerano, *Opt. Mater.*, 2018, **85**, 183–185.
31 J. Kischkat, S. Peters, B. Gruska, M. Semtsiv, M. Chashnikova, M. Klinkmüller, O. Fedosenko, S. Machulik, A. Aleksandrova, G. Monastyrskyi, Y. Flores and W. T. Masselink, *Appl. Opt.*, 2012, **51**, 6789–6798. Numerical values of n and k were accessed through the Refractive index database https://refractiveindex.info/ (accessed August 2021).
32 N. Gruhler, T. Yoshikawa, P. Rath, G. Lewes-Malandrakis, E. Schmidhammer, C. Nebel and W. H. P. Pernice, *Phys. Status Solidi A*, 2016, **213**, 2075–2080.
33 C. Chen, A. Xu, X. Li, M. Jiang, T. Xu, B. Yan and X. Hu, *Phys. Status Solidi A*, 2020, **217**, 2000076.
34 S. Mandal, C. Yuan, F. Massabuau, J. W. Pomeroy, J. Cuenca, H. Bland, W. Thomas, D. Wallis, T. Batten, D. Morgan, R. Oliver, M. Kuball and O. A. Williams, *ACS Appl. Mater. Interfaces*, 2019, **11**, 40826–40834.
35 G. F. Iriarte, F. Engelmark, I. V. Katardjiev, V. Plessky and V. Yantchev, *IEEE Trans. Ultrason., Ferroelectr., Freq. Control*, 2003, **50**, 1542–1547.
36 K. Fromell, P. Forsberg, M. Karlsson, K. Larsson, F. Nikolajeff and L. Baltzer, *Anal. Bioanal. Chem.*, 2012, **404**, 1643–1651.
37 1-D mode solver for dielectric multilayer slab waveguides, https://www.computational-photonics.eu/oms.html (accessed August 2021).
38 A. Oskooi, D. Roundy, M. Ibanescu, P. Bermel, J. D. Joannopoulos and S. G. Johnson, *Comput. Phys. Commun.*, 2010, **181**, 687–702.
39 G. M. Hale and M. R. Querry, *Appl. Opt.*, 1973, **12**, 555–563.
40 F. W. Dalby and H. H. Nielsen, *J. Chem. Phys.*, 1956, **25**, 934–940.
41 W. S. Benedict, H. H. Claassen and J. H. Shaw, *J. Res. Natl. Bur. Stand. (U. S.)*, 1952, **49**, 91–132.
42 I. Litvak, Y. Anker and H. Cohen, *RSC Adv.*, 2018, **8**, 28472–28479.
43 S. Vahur, A. Teearu, P. Peets, L. Joosu and I. Leito, *Anal. Bioanal. Chem.*, 2016, **408**, 3373–3379.
44 J.-J. Max and C. Chapados, *J. Chem. Phys.*, 2003, **119**, 5632–5643.
45 ICH Quality Guidelines 2005, Q2(R1).
46 S. Boyd and J. Kirkwood, Quantitative analysis using ATR-FTIR Spectroscopy, Agilent Technologies application note si-01374, https://www.agilent.com/cs/library/applications/si-1374.pdf, accessed April, 2021.
47 R. Soref, *Nat. Photonics*, 2010, **4**, 495–497.